

Cite this: *Mater. Adv.*, 2023,  
4, 6730

# Maskless patterning of metal nanoparticles and silicon nanostructures by a droplet deposition and etching process

Chia-Wen Tsao \* and Ping-Chin Shen

This paper introduces a droplet-based method to deposit metal nanoparticles (named: droplet deposition) and etch silicon surfaces creating silicon nanostructures (named: droplet etching). The droplet deposition and etching process is a simple and cost-effective method that only requires a pipette tip for silver and gold nanoparticle coating and fabrication of silicon nanostructures. Besides, it also eliminates the need for mask designs or other fabrication facilities, simplifying the nanoparticle and silicon nanostructure patterning process. For the noble metal nanoparticle coating by droplet deposition, we investigate the influence of various process parameters such as metal ion concentration, hydrofluoric acid concentration, deposition time, and temperature effects on the resulting nanoparticle plating. And for silicon nanostructure creation, we use the droplet etching technique that selectively etches the silicon in regions where metal nanoparticles have been deposited while other regions remain unaffected and well-preserved. Finally, we demonstrate the capability of hand-writing geometric patterning, transferring pre-defined patterns by shadow masking and mass production for droplet deposition and etching using a multi-channel (8-channel) pipette.

Received 8th July 2023,  
Accepted 16th November 2023

DOI: 10.1039/d3ma00380a

rsc.li/materials-advances

## 1. Introduction

Over the past few decades, the nano-texturing of silicon surfaces has gained significant attention due to its extensive applicability in a variety of fields.<sup>1–3</sup> This involves coating metal nanoparticles or creating porous/wire-shaped nanostructures on silicon surfaces. The deposition of the nanoparticle layers typically employs dry deposition facilities like e-beam,<sup>4</sup> thermal evaporators,<sup>5</sup> or sputtering apparatus.<sup>6</sup> And generation of silicon nanostructures can be generally achieved *via* top-down methods like anisotropic wet chemical etching,<sup>7</sup> laser-assisted etching,<sup>8</sup> plasma etching,<sup>9</sup> reactive ion etching,<sup>10</sup> deep reactive ion etching,<sup>11</sup> or bottom-up methods, like chemical vapor deposition (CVD),<sup>12,13</sup> physical vapor deposition (PVD)<sup>14</sup> or laser ablation synthesis<sup>15</sup> approaches.

While these deposition and etching facilities offer precise control over thickness and uniformity, they are usually costly to acquire and maintain, thereby limiting accessibility for use. As a solution, researchers have proposed the use of simple processes such as electroless plating<sup>16</sup> or the metal-assisted chemical etching (MACE)<sup>17</sup> process to create metal nanoparticles or silicon nanostructures. Owing to their straightforward and efficient fabrication setups that don't necessitate the preparation

and setup of a galvanic etching cell to generate nanostructured silicon surfaces,<sup>18</sup> both electroless plating and MACE have emerged as appealing methods for nanoparticle deposition<sup>16</sup> or silicon nanostructure fabrication in various fields including micro-electrical mechanical systems,<sup>19,20</sup> biosensors,<sup>21,22</sup> solar cells,<sup>23,24</sup> energy storage,<sup>25,26</sup> mass spectrometry,<sup>27,28</sup> *etc.*

Both electroless plating and the etching process typically involve immersing the entire silicon substrate in the plating electrolyte or etching solution. To pattern the metal or silicon nanostructure layer by electroless plating or etching, selective masking techniques can be applied to protect specific areas from coating, resulting in a patterned region on the silicon surface. This is usually done by a standard photolithography,<sup>29</sup> electron beam lithography,<sup>30</sup> or soft lithography<sup>31</sup> process. Nevertheless, these lithography-based techniques typically require lithography facilities or masks to generate the patterns, which can be costly and time-consuming. Alternative maskless techniques for pattern generation, such as using self-assembly,<sup>32,33</sup> a magnetic field,<sup>34</sup> or direct laser machining<sup>35</sup> are being developed to address these limitations. While these techniques offer some advantages, they still require additional steps or specialized equipment. Therefore, there is a need to develop a simple, low-cost method for generating metal nanoparticles or nanostructures.

In this paper, we present a new electroless plating method to deposit silver and gold nanoparticles on a silicon substrate using droplets. Notably, this approach simplifies the process of

Department of Mechanical Engineering, National Central University, Taoyuan City, Taiwan. E-mail: cwtsao@ncu.edu.tw; Fax: +886-3-4254501; Tel: +886-3-4267343



generating metal nanoparticle patterns on a silicon surface without mask design or other additional steps. To create silicon nanostructures, we utilize this droplet method to locally etch the silicon *via* an etching process, whereby the etchant selectively etches the metal nanoparticle coated region while leaving other areas protected. In addition to its mask-free advantage, this droplet-based method is more cost-effective, requiring only a small amount of noble metal deposition reagent (a few microliters) and generating less hazardous waste during the process compared to commonly used fully immersive electroless plating methods.

## 2. Experiment

### 2.1 Materials and reagents

Hydrofluoric acid (concentration 49%), hydrogen peroxide (concentration 31%), acetone (concentration 100%), and isopropanol (concentration 99.8%) were purchased from BASF Corp (BASF Taiwan, Taipei, Taiwan). Ethanol (concentration 99.5%), methanol (concentration 99.9%), and water (HPLC grade) were purchased from J. T. Baker Chemical Company (Phillipsburg, NJ, USA). Silver nitrate (ACS, 99.9+%, metals basis) and sodium tetrachloroaurate(III) dihydrate (99.99%, metal basis, AU 49–50%) were purchased from Alfa Aesar (MA USA). A boron-doped P-Type wafer (4 inch, single side polished, test grade, resistivity: 1–10 Ohm·cm) was obtained from Advanced Furnace Systems Corp. (Tainan, Taiwan). Prior to metal deposition, the silicon wafer was cut into  $1 \times 1 \text{ cm}^2$  and cleaned with acetone and isopropyl alcohol, followed by rinsing with DI water using an ultrasonic bath to remove the silicon particles and surface contaminants. Gold and silver nanoparticle deposition solutions were prepared by dissolving 28.7 mg tetrachloroaurate(III) dihydrate and 12.3 mg silver nitrate in 26.1 mL HPLC water, respectively, in 3 minutes in an ultrasonic bath, and mixed with 10 mL HF (49%) solution as a deposition reagent. Polydimethylsiloxane (PDMS, SYLGARD™ 184) was purchased from Dow Corning Inc. (Atlanta, GA, USA). SU-8 3050 and SU-8 developer were purchased from MicroChem Corp. (Westborough, MA, USA).

### 2.2 Contact angle measurements

An automatic contact angle measurement system (OCA 15EC, DataPhysics Instruments, Filderstadt, Germany) was used to

measure the surface hydrophobicity. In each test, 2  $\mu\text{L}$  water was auto-pipetted onto the silicon surface, and the droplet image was captured and analyzed to calculate the contact angle.

### 2.3 Scanning electron microscope (SEM) image analysis

The SEM images were taken using a Hitachi FESEM (S-4300, Krefeld, Germany) at the Optical Sciences Center at National Central University, Taiwan. All samples were cut into  $0.5 \times 0.5 \text{ cm}^2$  wafers, and attached to the SEM holder to take the top and cross-section images.

## 3. Results and discussion

### 3.1 Metal nanoparticle plating and silicon nanostructure preparation by droplet deposition

The droplet deposition method is a straightforward process that involves using a pipette to extract a small amount of deposition or etchant solution onto the silicon substrate for the droplet deposition or droplet etching process. We first illustrate the droplet deposition process, shown in Fig. 1. The process begins with a bare silicon wafer and directly pipetting the deposition solution droplet onto the silicon surface. The droplet is left to stay for a couple of minutes, allowing for the electroless plating of noble metal nanoparticles such as Au and Ag onto the silicon surface. Subsequently, the whole substrate is subjected to immersion cleaning in a water beaker to remove the deposited droplets from the silicon surface. It is noted that the quality of the deposition can be directly influenced by the droplet removal process, given that the deposition solution is hydrophilic to the silicon surface at an angle of approximately 35 degrees. In our tests, we attempted to remove the droplet directly by rinsing with water or by drying *via*  $\text{N}_2$  gun blowing; but these methods resulted in deposition solution residues leaving deposition marks on the surface. As a result, we opted for the immersion cleaning approach for 5 minutes to rinse the deposition solution from the silicon wafer thoroughly. Finally, the coated substrate is removed from the water beaker, and then  $\text{N}_2$  blow-dried to complete the nanoparticle plating process.

Due to direct contact between the droplet and the silicon surface, the nanoparticle plating patterns become intrinsically correlated with the contact region between the droplet and the

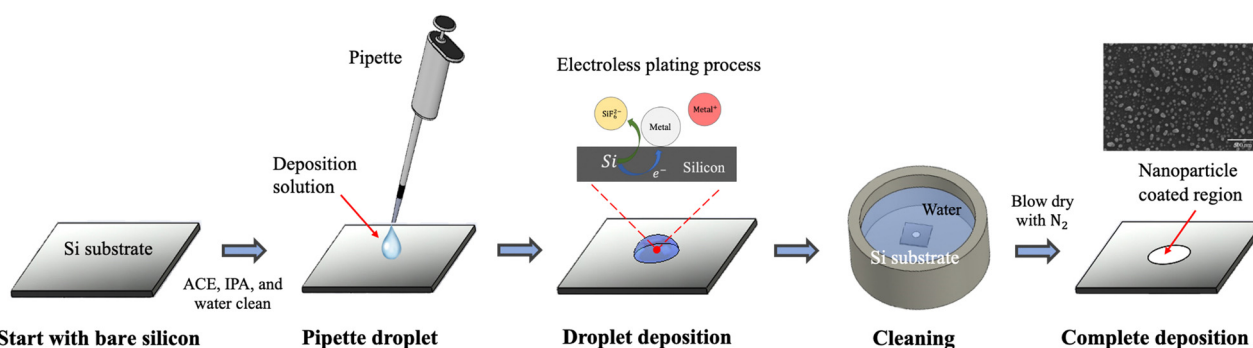


Fig. 1 Schematic illustration of the droplet deposition process.



silicon wafer. This contact enables selective deposition of nanoparticles onto the contact region, which determines the pattern of nanoparticle plating. To ensure high-quality nanoparticle plating patterns, precise control over the deposition conditions is essential. In the following discussion, we explore the impact of various parameters, including metal ion concentration, temperature, hydrofluoric acid concentration, deposition time, and temperature effects, in order to determine the optimal deposition conditions.

**3.1.1 The effect of metal ion concentration on metal nanoparticle plating.** The concentration of metal ions in the plating solution is one of the most critical factors in the droplet-based deposition process as it determines the amount of metal nanoparticles deposited onto the silicon substrate. To investigate the impact of metal ion concentration on deposition, we tested silver and gold plating solutions at varying concentrations, including 1 mM, 2 mM, 4 mM, and 8 mM. The concentration of HF was maintained at a fixed concentration of 8 M with 1  $\mu$ L droplet volume operating at room temperature.

The SEM images in Fig. 2 demonstrate the Ag (a)–(d) and Au (e)–(h) droplet deposition results at varying metal ion concentrations of 1 mM (a), (e), 2 mM (b), (f), 4 mM (c), (g) and 8 mM (d), (h). As the concentration of metal ions increases, the size and coverage rate of deposited metal nanoparticles also increase. The Ag and Au nanoparticle morphology changes with increased concentration. The silver deposition exhibits a three-dimensional dendritic or net-like morphology, while gold deposition tends to grow in a two-dimensional film morphology. Due to the stronger interaction between gold and silicon and heteroepitaxial growth, gold clusters follow the Stranski–Krastanov growth mode. In this mode, gold initially forms two-dimensional planar monolayers.<sup>36,37</sup> On the other hand, silver forms small clusters on the surface following the Volmer–Weber growth mode. Due to the agglomeration of silver clusters and strong anisotropic growth, silver follows a diffusion-limited aggregation model to grow and forms three-dimensional dendritic structures.<sup>38,39</sup>

The particle size distribution and deposition coverage are summarized in Fig. 3. It clearly shows that both the size and surface coverage of deposited metal nanoparticles grow proportionally with increasing ion concentrations. At a low metal ion concentration of 1 mM, the majority of metal nanoparticles are found to be distributed within a  $0\text{--}1 \times 10^{-3} \mu\text{m}^2$  range. At a high metal ion concentration of 8 mM, there is noticeable growth in large metal particles of both silver and gold, with sizes exceeding  $5 \times 10^{-3} \mu\text{m}^2$ . Correspondingly, the surface coverage shows an increase from 23.4% to 41% for silver and from 34.5% to 80.1% for gold. This difference is attributed to the distinct surface morphology between Ag and Au, illustrated in Fig. 2. Notably, gold nanoparticles exhibit a tendency to grow laterally under increased ion concentrations, leading to higher deposition coverages compared to silver deposition.

Additionally, the effects of metal ion concentration on deposition times were investigated. The experiments were conducted using three distinct deposition durations of 30, 60, and 90 seconds under conditions of 8 M HF and 4 mM ion concentrations. As displayed in Fig. 4, we observe growth in particle size with time for Ag droplet deposition. Gold exhibits more minor differences in deposition at three different time intervals than silver. This is presumably due to the high deposition coverage of gold; the number of active deposition sites available for metal ion attachment is relatively limited. This leads to a decrease in the deposition rate and shows little effect on Au droplet deposition conditions.

**3.1.2 The effect of HF concentration on metal nanoparticle plating.** To determine the optimal HF conditions for droplet deposition, we experimented with different HF concentrations for 4 M to 12 M. Fig. 5 shows the SEM images of silver and gold nanoparticles coated on the silicon surface by the droplet deposition with 4 M (a), (d), 8 M (b), (e), and 12 M (c), (f) HF concentrations. It can be observed from the figure that as the concentration of hydrofluoric acid increased, silver and gold showed difference. For silver nanoparticles, an increase in HF

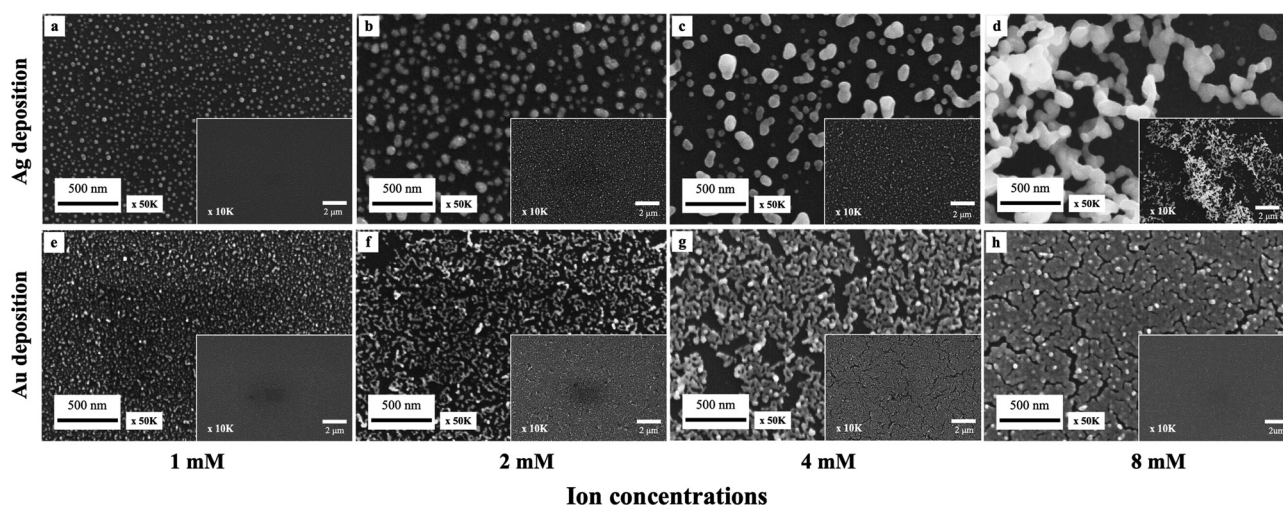


Fig. 2  $\times 50\text{k}$  and  $\times 10\text{k}$  (right-bottom) SEM images of silver (Ag) and gold (Au) nanoparticles by droplet deposition with 1 mM, 2 mM, 4 mM, and 8 mM ion concentrations. The HF concentration was 8 M, and the deposition time was 60 seconds.



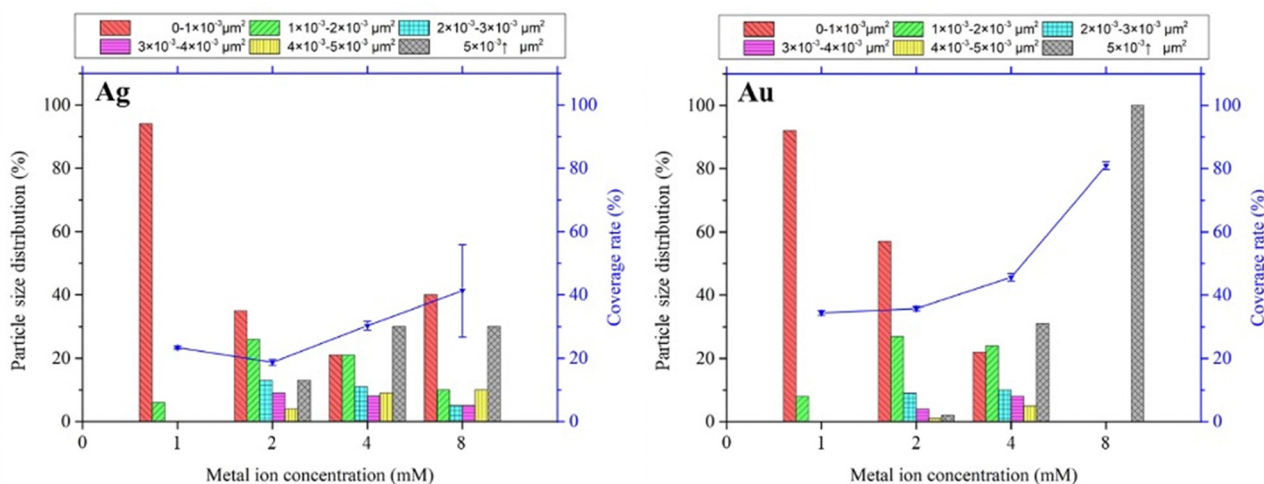


Fig. 3 Particle size distribution percentage (black color y-axis label) and coverage percentage (blue color y-axis label) for Ag and Au nanoparticle deposition with various metal ion concentrations. The particle size distribution % is defined as the ratio of the number of metal particles in each size segment to the total number of metal particles, and the coverage percentage is defined as the ratio of metal coverage area to the total area.

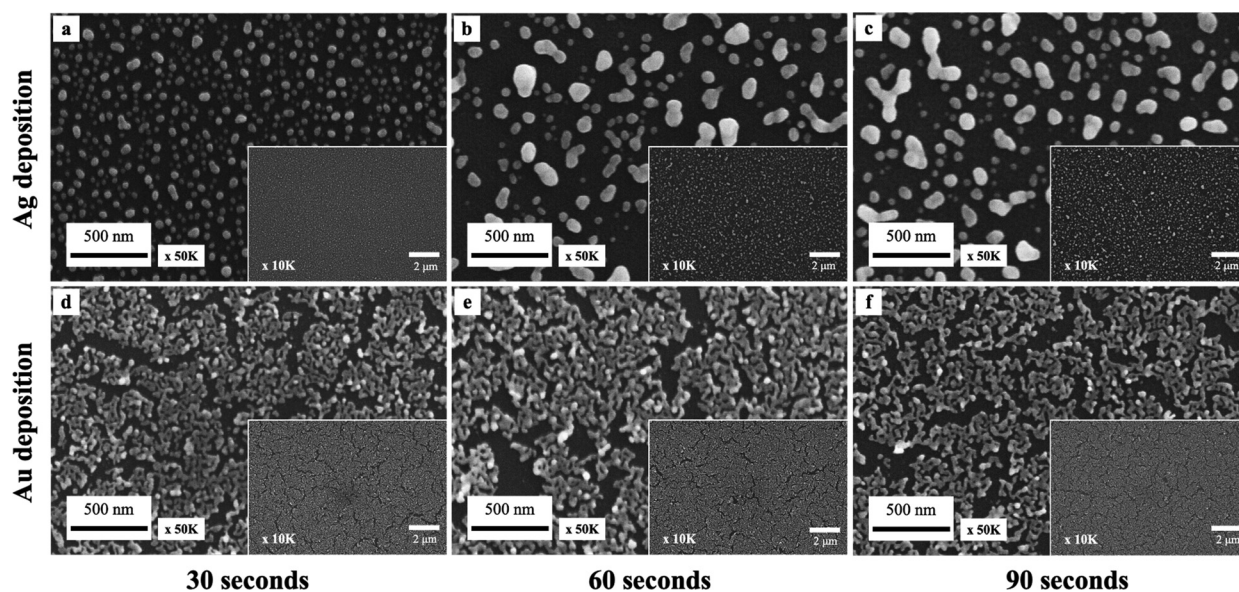
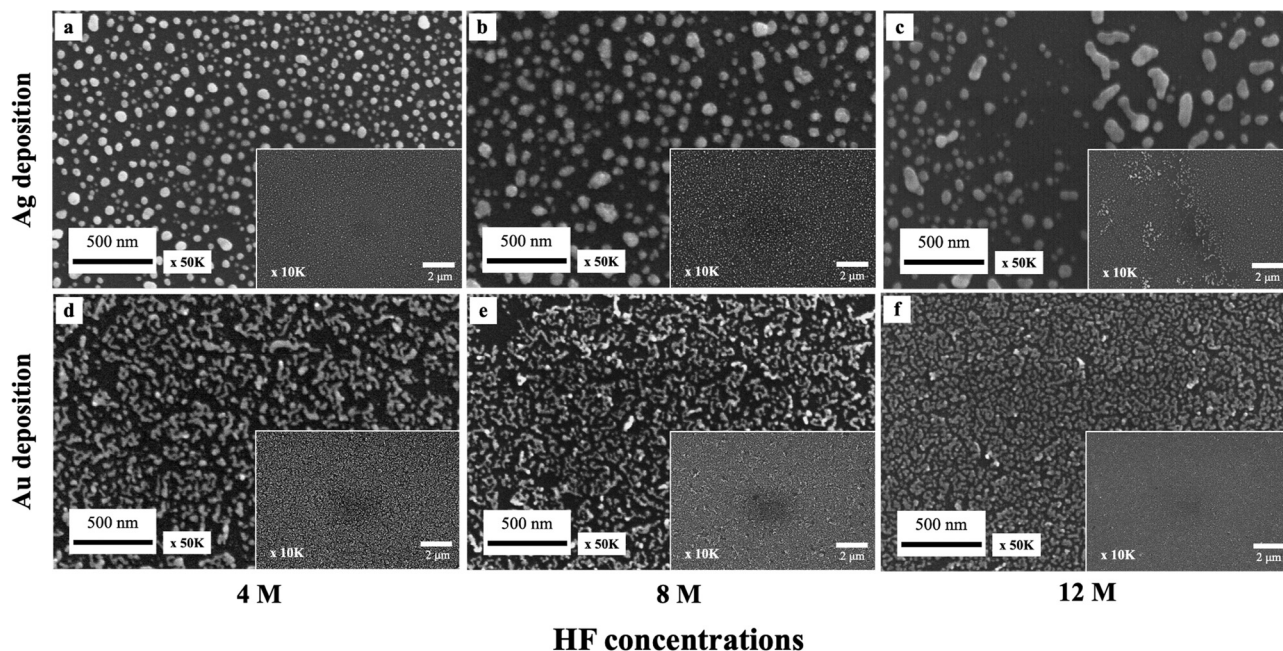


Fig. 4  $\times 50k$  and  $\times 10k$  (right-bottom) SEM images of silver (Ag) and gold (Au) nanoparticles by droplet deposition with 30, 60, and 90 seconds. The ion concentration was 4 mM, and the HF concentration was 8 M.

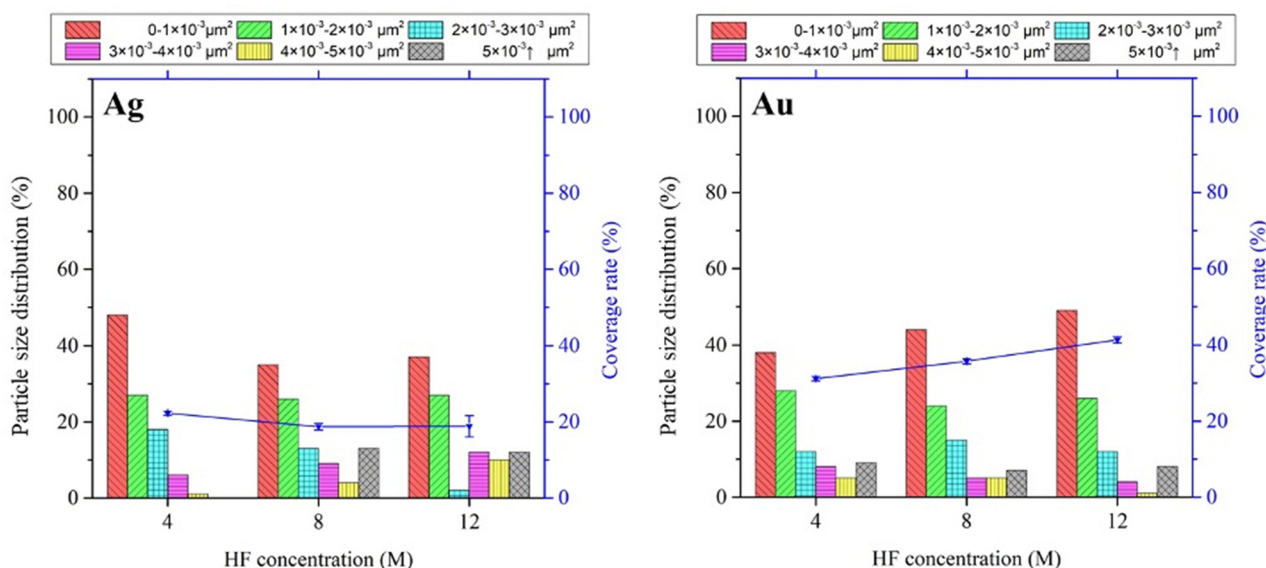
concentration induces growth into larger particles. In this process, HF serves as an etchant that dissolves the silicon substrate and releases electrons for deposition. Thereby, by increasing the concentration of hydrofluoric acid in the solution, the silicon etching rate can be increased, resulting in a higher concentration of electrons available for deposition into a bigger nanoparticle.<sup>40</sup> For gold droplet deposition, as it tends to grow towards a two-dimensional thin film in the lateral direction, an increase in HF concentration does not lead to larger particles but increases the coverage rate percentage from 31.2% to 41.3%. Considering the objective of achieving optimal deposition uniformity, we selected an 8 M HF concentration for the deposition conditions in subsequent tests.

**3.1.3 Effect of temperature on droplet deposition.** The droplet deposition method involves plating nanoparticles onto the silicon surface using only a few microliters of the deposition solution. Consequently, the droplet becomes prone to evaporation or temperature variations. To explore the thermal influence on droplet deposition, we carried out experiments at 60 °C and compared these results with those observed in a room temperature environment (20 °C) with 30 to 90 seconds deposition time. As illustrated in Fig. 6(a), it can be observed that under both silver and gold deposition conditions, the droplet positioned at the center does not significantly evaporate until 90 seconds. Conversely, at an elevated temperature of 60 °C, the deposition droplets begin to evaporate as early as





(a)



(b)

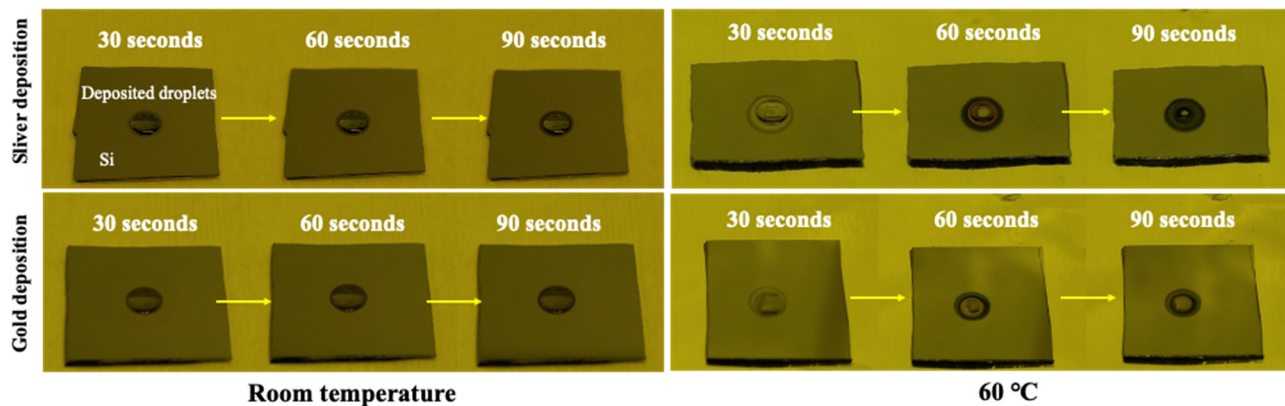
**Fig. 5** (a)  $\times 50k$  and  $\times 10k$  (right-bottom) SEM images of silver (Ag) and gold (Au) nanoparticles by droplet deposition with 4, 8, and 12 M concentrations. The ion concentration was 2 mM, and the HF concentration was 8 M. Deposition time is 60 seconds. (b) Particle size distribution percentage (black color y-axis label) and coverage percentage (blue color y-axis label) for Ag and Au nanoparticle deposition with various metal ion concentrations. The particle size distribution % is defined as the ratio of the number of metal particles in each size segment to the total number of metal particles, and the coverage percentage is defined as the ratio of metal coverage area to the total area.

30 seconds, leaving a small electroless deposition solution near the center by 90 seconds.

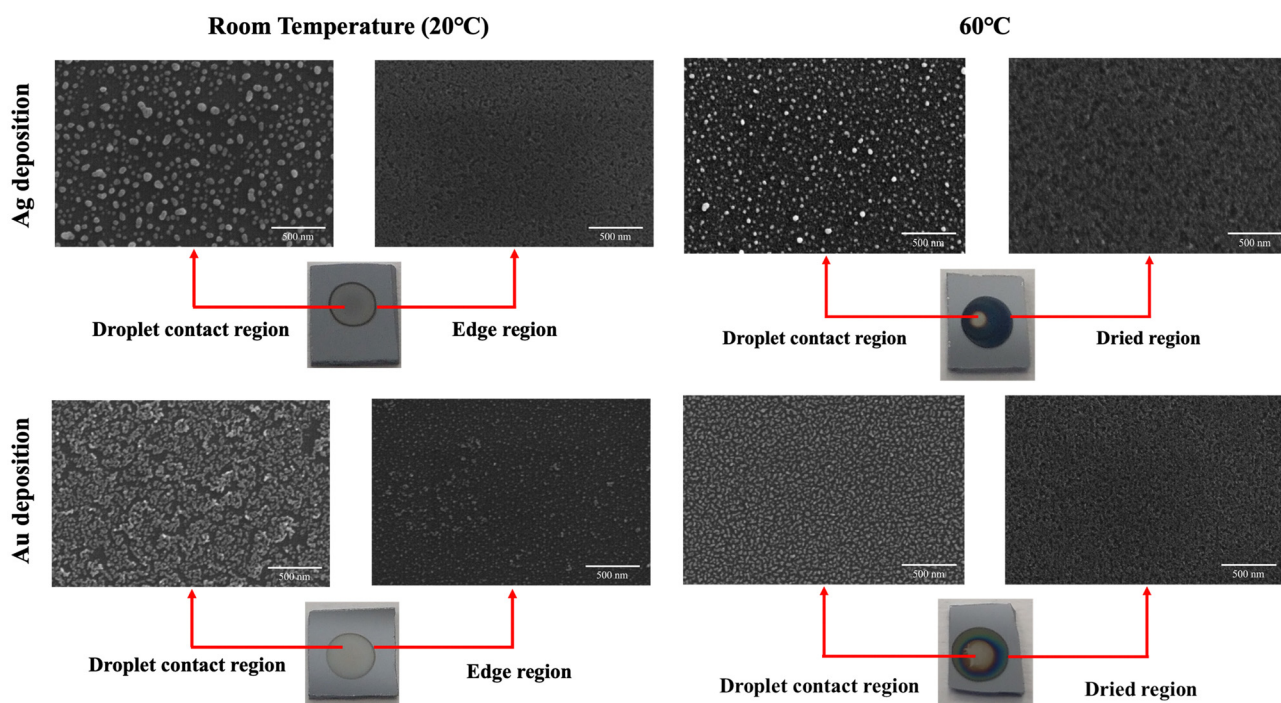
Referring to the SEM image depicted in Fig. 6(b), it can be discerned that under room temperature conditions, silver and gold are more uniformly deposited onto the silicon surface within the droplet contact area compared to that under the higher temperature conditions, with the exception of the droplet edge. Conversely, at 60 °C, the deposition droplet evaporates and concentrates towards the center at this elevated temperature, resulting in a

higher nanoparticle density at the droplet contact region, while the dried areas exhibit only a minimal nanoparticle presence on the surface. Furthermore, we observed an expansion of the edge etching region in the droplet deposition method as the deposition temperature increased. This phenomenon can be attributed to the reduction in droplet size due to evaporation, causing the dry region to be exposed to hydrofluoric acid etching before complete evaporation. We speculate that droplet evaporation has an adverse effect on droplet deposition, making it more challenging for metal ions to





(a)



(b)

Fig. 6 (a) Photographic images of droplet evaporation over time (30–90 seconds) at room and elevated 60 °C temperatures. (b) SEM images illustrating Ag and Au nanoparticle distribution on the silicon surface at room temperature and 60 °C by the droplet deposition method.

reach the edge region for deposition, resulting in non-uniform metal deposition under high temperature conditions. Therefore, it is important to control the droplet evaporation/condensation on the silicon surface if uniform droplet deposition is required. We suggested minimizing the possibility of droplet evaporation by lowering the deposition temperature or increasing the environmental humidity.

### 3.2 Nanostructured silicon surface fabrication by droplet etching

Following the deposition of noble metal nanoparticles, we employed MACE to create silicon nanostructures by the droplet

etching approach. This process differs from the conventional MACE practice, where noble metal-coated silicon substrates are fully immersed in the etching solution. This droplet etching method offers an advantage for the local etching of Ag/Au-coated regions without causing damage to the uncoated region. The droplet etching is demonstrated in Fig. 7. It begins with the deposition of the HF/H<sub>2</sub>O<sub>2</sub>/C<sub>2</sub>H<sub>5</sub>OH (volume ratio 5:1:5) etching solution onto the coated region and staying for a few minutes. Following this, the entire substrate is rinsed with methanol, and subsequently dried using an N<sub>2</sub> gun to fabricate the nanostructure pattern on the silicon surface.



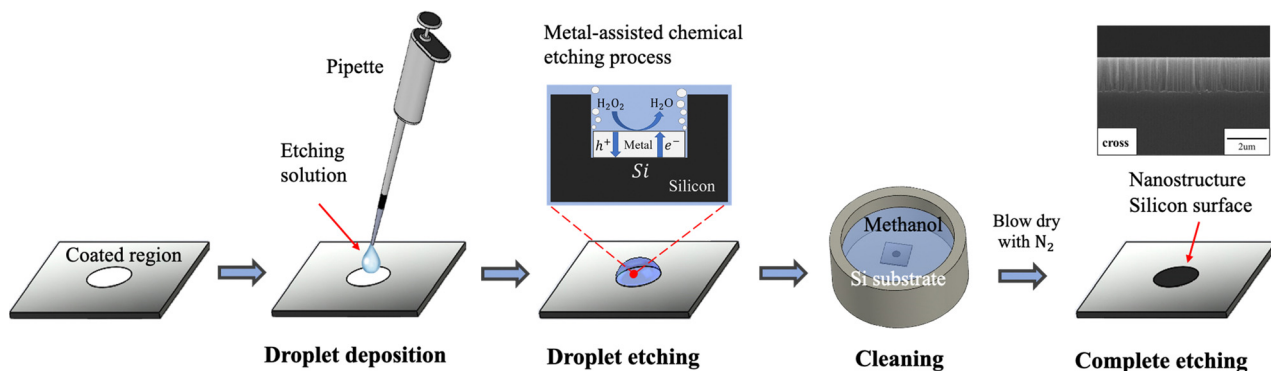


Fig. 7 Schematic illustration of the droplet etching process.

From the SEM images presented in Fig. 8, circular-shape silicon nanostructure patterns are generated by the droplet etching process. The Ag-coated substrate shows 0.1–0.8  $\mu\text{m}$  diameter and 0.6–2.7  $\mu\text{m}$  height pore-shape surface morphology. The Au-coated substrate shows 0.1–0.6  $\mu\text{m}$  diameter and 1.6–1.7  $\mu\text{m}$  height wire-shape surface morphology. For 1 minute etching time, as displayed in Fig. 8(a), the silicon nanostructure morphology, size, and length created by the droplet etching process are similar to those created using the conventional MACE process where the silicon substrate was fully immersed in the etching solution for a short etching time. An important distinguishing feature of the droplet etching process is its ability to confine etching to the Ag/Au-coated regions. This effectively leaves the silicon surface outside the droplet etching region unscathed and protected, ensuring the preservation of the base material's integrity. In contrast, full immersion MACE etching often results in the formation of numerous tiny pits dispersed across substrate areas that are not targeted for etching, as shown in Fig. 8(a). This demonstrates the advantages over the standard MACE process. It effectively prevents silicon surfaces outside the metal deposition area from being damaged by HF etching, making it particularly valuable for applications requiring a high degree of surface flatness, such as silicon bonding. Furthermore, the droplet etching process offers the advantage of selective etching in the desired metal deposition areas without the need for intricate masking techniques to protect the surface from being etched or damaged, which is typically associated with conventional MACE processes.

When extending the etching time to 20 minutes, as demonstrated in Fig. 8(b), distinct morphological differences become apparent between droplet etching and immersion etching. Although both the Ag- and Au-coated substrates present similar pore and wire-shaped surface morphologies, the immersion method tends to yield larger surface features compared to the droplet etching process. For Ag-coated substrates the pore shape surface was measured to have 0.9–2.1  $\mu\text{m}$  diameter and 3–15  $\mu\text{m}$  height. And for Au coated substrates, the pore shape surface was measured to have 0.8–1.5  $\mu\text{m}$  diameter and 18–44  $\mu\text{m}$  height. Since the droplet etching employs significantly less solution than the immersion method (1  $\mu\text{L}$  compared to  $\sim 200$  mL), it is plausible that, with the progression of the reaction, the overall HF and  $\text{H}_2\text{O}_2$  concentrations decrease over

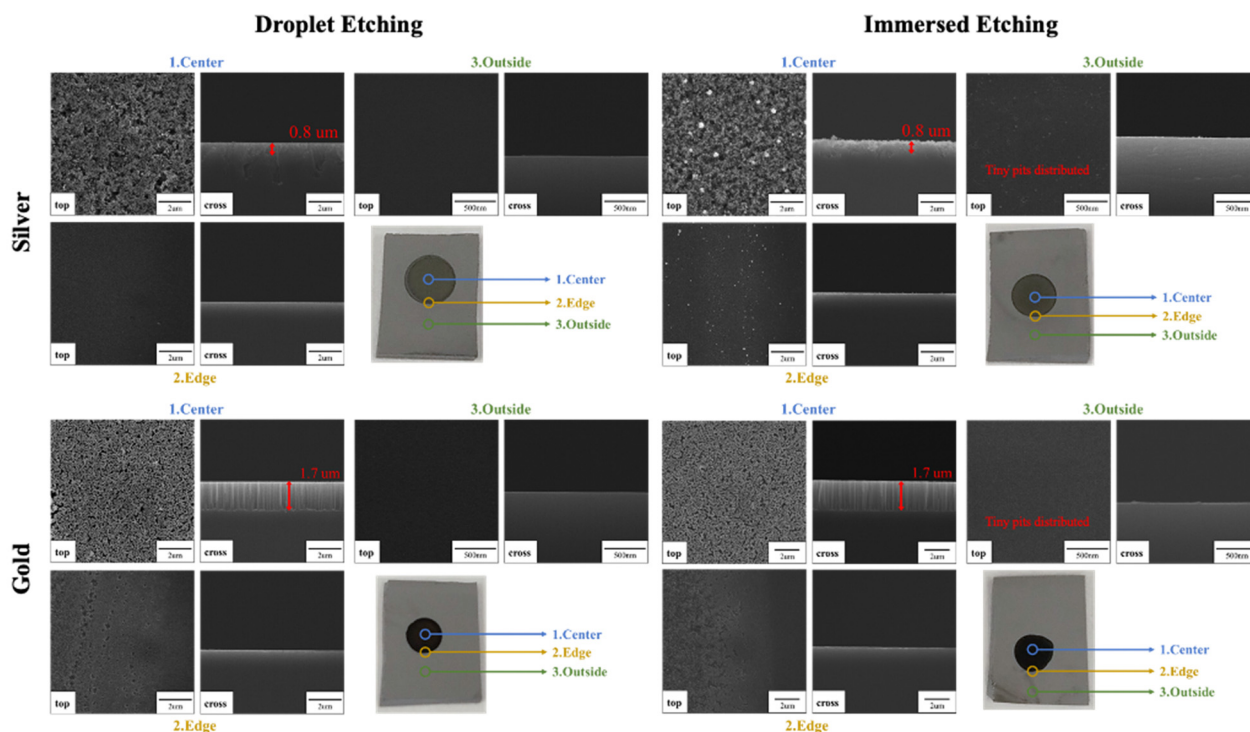
a long reaction time which decreases the etching rate in a small volume. Therefore, we observed surface morphology difference for more extended etching time conditions.

### 3.3 Maskless patterning of metal nanoparticles and porous silicon by the droplet deposition method

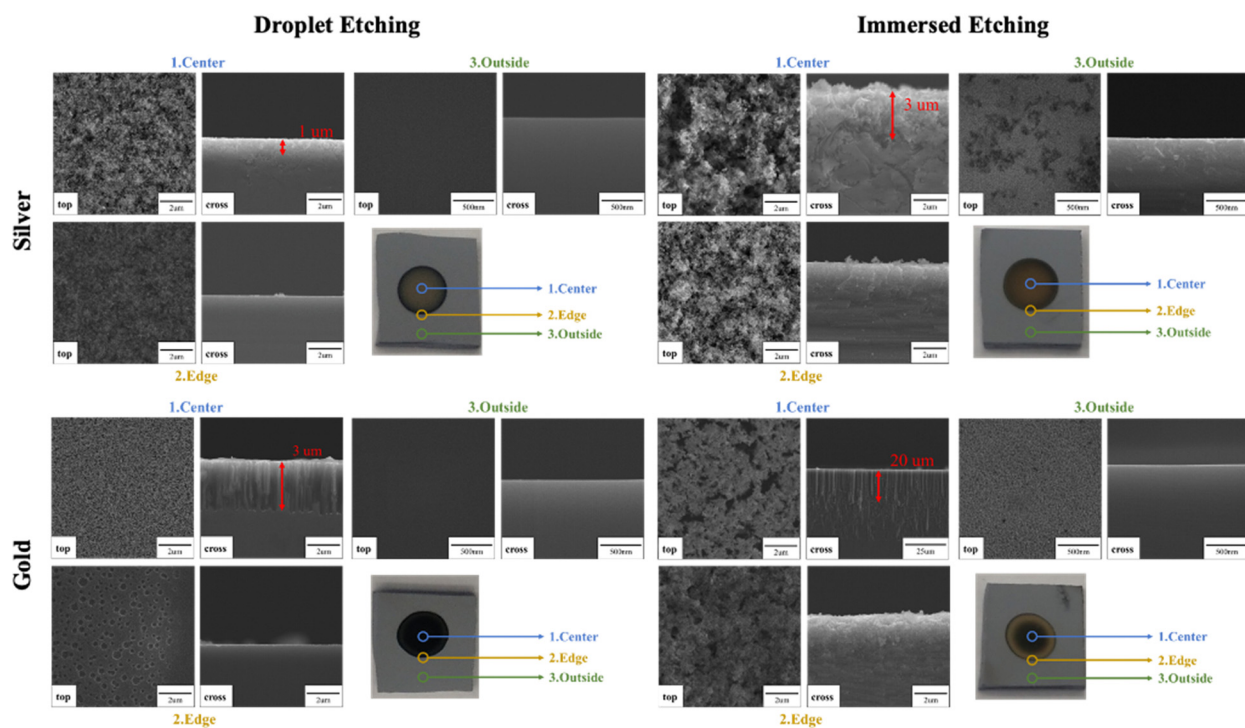
**3.3.1 Correlation between the droplet volume and pattern size.** Precise control of the droplet–silicon wafer contact region is essential to ensure high-quality nanoparticle plating as well as consequent silicon nanostructure patterns for this droplet deposition and etching approach. In the droplet deposition process, when a droplet comes into contact with a bare silicon surface, it spreads out due to its hydrophilic nature (contact angle:  $\sim 35$  degrees) which forms a circular shape pattern on the silicon surface. Thus, the size of the pattern is highly correlated with the volume of the droplet. Fig. 9 illustrates the relationship between droplet volumes ranging from 0.2 to 8  $\mu\text{L}$  and the corresponding deposition areas. For a 0.2  $\mu\text{L}$  droplet, the deposition size was measured to be  $1726 \pm 176 \mu\text{m}$ . As the deposition volume increases, the droplet size correspondingly expands, reaching  $5531 \pm 403 \mu\text{m}$ . This trend underscores the importance of controlling the droplet volume in achieving the desired pattern sizes. Consequently, through manipulating droplet volumes, we can regulate and customize pattern dimensions effectively for different applications.

**3.3.2 Pattern generation and multi-channel deposition by the droplet deposition and etching process.** In addition to droplet volume-based size control as discussed previously, this droplet-based technique also offers the ability to manually deposit or ‘hand-write’ a variety of nanoparticle geometries, such as  $2 \times 3$  array patterns, straight lines, triangles, squares, circles, or even text directly onto silicon surfaces. Fig. 10(a) demonstrates the resulting silicon nanostructure geometries generated by the droplet deposition and etching process. Alternatively, we can employ a shadow mask layer to transfer pre-designed patterns onto the silicon surface by restricting the deposited droplets. As depicted in Fig. 10(b), the PDMS masking layer can be created through straightforward cutting or by casting from an SU-8 micromold. Following the fabrication of the mask layer, the PDMS mask layer is affixed onto the silicon substrate. Subsequently, droplet deposition is performed onto the mask layer to transfer the predetermined pattern onto the





(a)



(b)

Fig. 8 Etching for (a) 1 minute and (b) 20 minutes. The silver and gold nanoparticle coating for this droplet etching test is 8 M HF 2 mM ion concentration, deposition time: 90 seconds, room temp.

silicon surface. Post the droplet deposition phase, the formation of silicon nanostructure patterns can be generated

through droplet-based MACE etching procedures which is displayed in the Fig. 10(b) bottom image.



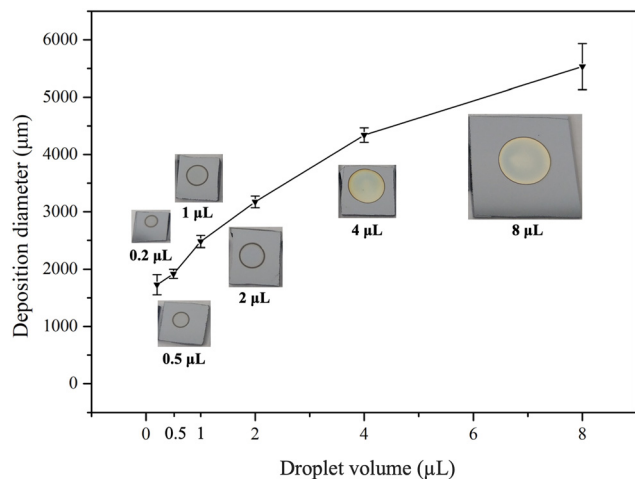


Fig. 9 Correlation between droplet volume and resultant pattern size on the silicon surface by droplet deposition. The deposition conditions for this experiment: 8 M HF concentration, 2 mM metal ion concentration, room temperature environment, and 90 seconds deposition time.

Another advantage of the droplet deposition method is its compatibility with commercially available droplet deposition systems or pipettes. In our earlier discussions, we utilized a single-channel pipette to examine the influence of various droplet deposition process parameters. However, when larger-scale depositions are required, multi-channel pipette tips can be used to pattern droplet arrays with high throughput. In addition, these tips are not confined to depositing a one-type deposition solution. Instead, each pipette tip can act as an individual deposition site, depositing various conditions on the substrate in a single run. As shown in Fig. 10(c), we demonstrate high-throughput microdroplet deposition using an 8-channel pipette (CAPP C200-8). In this test, the eight droplets contained four different types of deposition solutions (two droplets for 4 mM Ag, 4 mM Au, 1 mM Ag, and 1 mM Au). This allows the deposition of distinct coating reagents on the surface silicon in a single pipette run. These multi-channel approaches presented the flexibility and the scalability of the droplet deposition method marking the droplet deposition/etching method as a potential tool in nanotechnology research.

## 4. Conclusions

In this research, we have successfully demonstrated a novel methodology for maskless patterning of noble metal nanoparticles and silicon nanostructure fabrication *via* the droplet deposition and etching process. For the droplet deposition, we investigated various deposition parameters for silver and gold nanoparticle deposition. The results showed that metal ion concentration has a profound impact on nanoparticle deposition; both silver deposition and gold deposition show increasing nanoparticle size and coverage rate with increasing metal ion concentration. Given the droplet's small volume, deposition at room temperature was found to be preferable to ensure a uniform nanoparticle distribution. In contrast, at elevated

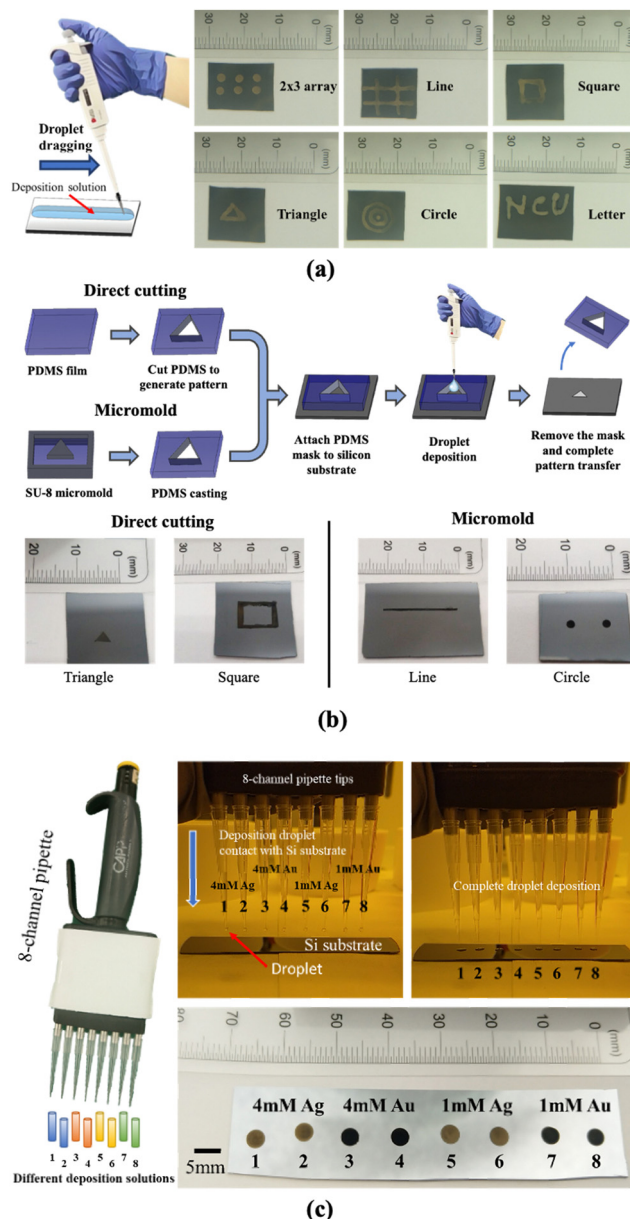


Fig. 10 Demonstration of the droplet deposition and droplet MACE etching by (a) hand-writing, (b) using PDMS as a masking layer, and (c) high-throughput patterning (8 patterns) generation with an 8-channel pipette tip.

temperatures above 60 °C, evaporation occurred, leading to a concentrated nanoparticle coating.

After nanoparticle deposition, we utilized the droplet etching method to locally etch silicon, creating silicon nanostructure patterns. This localized etching process ensures the protection of uncoated regions, showing another significant advantage of this method. In this study, we selected Ag and Au as noble metals in the proposed droplet-based MACE process to produce high aspect ratio porous silicon microstructures. Other metals such as Pt,<sup>41</sup> Cu<sup>42</sup> and Ni<sup>43</sup> can also be applied in this droplet-based approach to generate porous-shape (Pt) and pit or inverted pyramid shape (Cu and Ni) morphologies.



Finally, we use hand-writing and shadow mask methods to create various geometries and patterns on the silicon surface, and also demonstrated that the droplet deposition and etching method is fully compatible with commercially available droplet deposition or pipette systems, including both single-channel and multi-channel (8-channel) pipettes, as demonstrated in this paper. In the future, for industrial-level applications or higher fabrication throughput demands, automated 96/384-well/droplet high throughput electronic pipette systems can be used for more precise, controllable, and mass-produced droplet deposition, creating metal nanoparticles on silicon surfaces or porous silicon patterns for various applications.

## Conflicts of interest

There are no conflicts to declare.

## Acknowledgements

The authors would like to thank the National Science and Technology Council, Taiwan (NSTC), for financially supporting this project (grant number (NSTC 111-2221-E-008-MY3)).

## References

- 1 F. A. Harraz, Porous silicon chemical sensors and biosensors: A review, *Sens. Actuators, B*, 2014, **202**, 897–912, DOI: [10.1016/j.snb.2014.06.048](https://doi.org/10.1016/j.snb.2014.06.048).
- 2 G. J. Zhang and Y. Ning, Silicon nanowire biosensor and its applications in disease diagnostics: A review, *Anal. Chim. Acta*, 2012, **749**, 1–15, DOI: [10.1016/j.aca.2012.08.035](https://doi.org/10.1016/j.aca.2012.08.035).
- 3 Y. Yang, *et al.*, A review on silicon nanowire-based anodes for next-generation high-performance lithium-ion batteries from a material-based perspective, *Sustainable Energy and Fuels*, 2020, **4**(4), 1577–1594, DOI: [10.1039/c9se01165j](https://doi.org/10.1039/c9se01165j).
- 4 A. Khabari, F. K. Urban, III, P. Griffiths, I. Petrov, Y.-W. Kim and C. Bungay, Nanoparticle beam formation and investigation of gold nanostructured films, *J. Vac. Sci. Technol., B: Microelectron. Nanometer Struct. – Process., Meas., Phenom.*, 2003, **21**(6), 2313–2318, DOI: [10.1116/1.1615985](https://doi.org/10.1116/1.1615985).
- 5 D. Gaspar, *et al.*, Influence of the layer thickness in plasmonic gold nanoparticles produced by thermal evaporation, *Sci. Rep.*, 2013, **3**(1), 1469, DOI: [10.1038/srep01469](https://doi.org/10.1038/srep01469).
- 6 N. Baig, I. Kammakakam and W. Falath, Nanomaterials: a review of synthesis methods, properties, recent progress, and challenges, *Mater. Adv.*, 2021, **2**(6), 1821–1871, DOI: [10.1039/D0MA00807A](https://doi.org/10.1039/D0MA00807A).
- 7 M. Y. Arafat, M. A. Islam, A. W. B. Mahmood, F. Abdullah, T. S. Kiong and N. Amin, Study of Black Silicon Wafer through Wet Chemical Etching for Parametric Optimization in Enhancing Solar Cell Performance by PC1D Numerical Simulation, *Crystals*, 2021, **11**(8), 881, DOI: [10.3390/cryst11080881](https://doi.org/10.3390/cryst11080881).
- 8 N. H. Harb and F. A. H. Mutlak, Production and characterization of porous silicon *via* laser-assisted etching: Effect of gamma irradiation, *Optik*, 2021, **246**, 167800, DOI: [10.1016/j.ijleo.2021.167800](https://doi.org/10.1016/j.ijleo.2021.167800).
- 9 A. Smyrnakis, E. Almpanis, V. Constantoudis, N. Papanikolaou and E. Gogolides, Optical properties of high aspect ratio plasma etched silicon nanowires: fabrication-induced variability dramatically reduces reflectance, *Nanotechnology*, 2015, **26**(8), 085301, DOI: [10.1088/0957-4484/26/8/085301](https://doi.org/10.1088/0957-4484/26/8/085301).
- 10 A. D. Refino, *et al.*, Versatilely tuned vertical silicon nanowire arrays by cryogenic reactive ion etching as a lithium-ion battery anode, *Sci. Rep.*, 2021, **11**(1), 19779, DOI: [10.1038/s41598-021-99173-4](https://doi.org/10.1038/s41598-021-99173-4).
- 11 Y. J. Hung, S. L. Lee, B. J. Thibeault and L. A. Coldren, Fabrication of Highly Ordered Silicon Nanowire Arrays With Controllable Sidewall Profiles for Achieving Low-Surface Reflection, *IEEE J. Sel. Top. Quantum Electron.*, 2011, **17**(4), 869–877, DOI: [10.1109/Jstqe.2010.2068540](https://doi.org/10.1109/Jstqe.2010.2068540).
- 12 R. A. Puglisi, *et al.*, Chemical Vapor Deposition Growth of Silicon Nanowires with Diameter Smaller Than 5 nm, *ACS Omega*, 2019, **4**(19), 17967–17971, DOI: [10.1021/acsomega.9b01488](https://doi.org/10.1021/acsomega.9b01488).
- 13 A. Colli, *et al.*, Thermal and chemical vapor deposition of Si nanowires: Shape control, dispersion, and electrical properties, *J. Appl. Phys.*, 2007, **102**(3), 034302, DOI: [10.1063/1.2764050](https://doi.org/10.1063/1.2764050).
- 14 L. Wang, X. Zhang, S. Zhao, G. Zhou, Y. Zhou and J. Qi, Synthesis of well-aligned ZnO nanowires by simple physical vapor deposition on c-oriented ZnO thin films without catalysts or additives, *Appl. Phys. Lett.*, 2005, **86**(2), 024108, DOI: [10.1063/1.1851607](https://doi.org/10.1063/1.1851607).
- 15 N. Fukata, T. Oshima, T. Tsurui, S. Ito and K. Murakami, Synthesis of silicon nanowires using laser ablation method and their manipulation by electron beam, *Sci. Technol. Adv. Mater.*, 2005, **6**(6), 628–632, DOI: [10.1016/j.stam.2005.06.015](https://doi.org/10.1016/j.stam.2005.06.015).
- 16 A. Lahiri and S. I. Kobayashi, Electroless deposition of gold on silicon and its potential applications: review, *Surf. Eng.*, 2016, **32**(5), 321–337, DOI: [10.1179/1743294415Y.0000000060](https://doi.org/10.1179/1743294415Y.0000000060).
- 17 H. Han, Z. Huang and W. Lee, Metal-assisted chemical etching of silicon and nanotechnology applications, *Nano Today*, 2014, **9**(3), 271–304, DOI: [10.1016/j.nantod.2014.04.013](https://doi.org/10.1016/j.nantod.2014.04.013).
- 18 X. Li and P. W. Bohn, Metal-assisted chemical etching in HF/H<sub>2</sub>O(2) produces porous silicon, *Appl. Phys. Lett.*, 2000, **77**(16), 2572–2574.
- 19 N. Van Toan, X. Wang, N. Inomata, M. Toda, I. Voiculescu and T. Ono, Low Cost and High-Aspect Ratio Micro/Nano Device Fabrication by Using Innovative Metal-Assisted Chemical Etching Method, *Adv. Eng. Mater.*, 2019, **21**(8), 1900490, DOI: [10.1002/adem.201900490](https://doi.org/10.1002/adem.201900490).
- 20 O. J. Hildreth and D. R. Schmidt, Vapor Phase Metal-Assisted Chemical Etching of Silicon, *Adv. Funct. Mater.*, 2014, **24**(24), 3827–3833, DOI: [10.1002/adfm.201304129](https://doi.org/10.1002/adfm.201304129).
- 21 R. F. Balderas-Valadez, V. Agarwal and C. Pacholski, Fabrication of porous silicon-based optical sensors using metal-assisted chemical etching, *RSC Adv.*, 2016, **6**(26), 21430–21434, DOI: [10.1039/C5RA26816H](https://doi.org/10.1039/C5RA26816H).
- 22 V. Solis-Tinoco, S. Marquez, B. Sepulveda and L. M. Lechuga, Fabrication of well-ordered silicon nanopillars embedded in a microchannel *via* metal-assisted chemical etching: a route



- towards an opto-mechanical biosensor, *RSC Adv.*, 2016, **6**(88), 85666–85674, DOI: [10.1039/c6ra15485a](https://doi.org/10.1039/c6ra15485a).
- 23 C. Huo, *et al.*, Metal-Assisted Chemical Etching of Silicon in Oxidizing HF Solutions: Origin, Mechanism, Development, and Black Silicon Solar Cell Application, *Adv. Funct. Mater.*, 2020, **30**(52), 2005744, DOI: [10.1002/adfm.202005744](https://doi.org/10.1002/adfm.202005744).
- 24 S. D. Wang, S. Y. Chen, S. P. Hsu, C. Y. Liao and W. Y. Hsu, Ag and Cu metal-assisted chemical etching for diamond-wire-sawn single-crystalline silicon solar cell, *Appl. Surf. Sci.*, 2022, **578**, 152050, DOI: [10.1016/j.apsusc.2021.152050](https://doi.org/10.1016/j.apsusc.2021.152050).
- 25 J. H. Li, N. V. Toan, Z. Q. Wang and T. Ono, Metal-assisted-chemical-etching of silicon nanowires for templating 3D graphene growth towards energy storage in microsystems, *J. Micromech. Microeng.*, 2019, **29**(5), 055007, DOI: [10.1088/1361-6439/ab0b2f](https://doi.org/10.1088/1361-6439/ab0b2f).
- 26 W. McSweeney, H. Geaney and C. O'Dwyer, Metal-assisted chemical etching of silicon and the behavior of nanoscale silicon materials as Li-ion battery anodes, *Nano Res.*, 2015, **8**(5), 1395–1442, DOI: [10.1007/s12274-014-0659-9](https://doi.org/10.1007/s12274-014-0659-9).
- 27 C. W. Tsao and Z. J. Yang, High Sensitivity and High Detection Specificity of Gold-Nanoparticle-Grafted Nanostructured Silicon Mass Spectrometry for Glucose Analysis, *ACS Appl. Mater. Interfaces*, 2015, **7**(40), 22630–22637, DOI: [10.1021/acsami.5b07395](https://doi.org/10.1021/acsami.5b07395).
- 28 J. J. Thomas, Z. Shen, J. E. Crowell, M. G. Finn and G. Siuzdak, Desorption/ionization on silicon (DIOS): A diverse mass spectrometry platform for protein characterization, *Proc. Natl. Acad. Sci. U. S. A.*, 2001, **98**(9), 4932–4937, DOI: [10.1073/pnas.081069298](https://doi.org/10.1073/pnas.081069298).
- 29 B. H. Liu, F.-Y. Liao and J.-H. Chen, Design, fabrication, and characterization of electroless Ni-P alloy films for micro heating devices, *Thin Solid Films*, 2013, **537**, 263–268, DOI: [10.1016/j.tsf.2013.04.136](https://doi.org/10.1016/j.tsf.2013.04.136).
- 30 F. Gentile, *et al.*, Electroless deposition of metal nanoparticle clusters: Effect of pattern distance, *J. Vac. Sci. Technol. B*, 2014, **32**(3), 031804, DOI: [10.1116/1.4870058](https://doi.org/10.1116/1.4870058).
- 31 H. Lim, J. H. Noh, D. G. Choi, W. D. Kim and R. Maboudian, A simple soft lithographic nanopatterning of gold on gallium arsenide *via* galvanic displacement, *J. Nanosci. Nanotechnol.*, 2010, **10**(8), 5020–5026, DOI: [10.1166/jnn.2010.2390](https://doi.org/10.1166/jnn.2010.2390).
- 32 S. B. Ulapane, N. J. B. Kamathewatta, A. K. Borkowski, S. J. Steuart and C. L. Berrie, Periodic Silver and Gold Nanodot Array Fabrication on Nanosphere Lithography-Based Patterns Using Electroless Deposition, *J. Phys. Chem. C*, 2020, **124**(28), 15646–15655, DOI: [10.1021/acs.jpcc.0c05247](https://doi.org/10.1021/acs.jpcc.0c05247).
- 33 S. B. Ulapane, N. J. B. Kamathewatta, H. M. Ashberry and C. L. Berrie, Controlled Electroless Deposition of Noble Metals on Silicon Substrates Using Self-Assembled Monolayers as Molecular Resists To Generate Nanopatterned Surfaces for Electronics and Plasmonics, *ACS Appl. Nano Mater.*, 2019, **2**(11), 7114–7125, DOI: [10.1021/acsanm.9b01641](https://doi.org/10.1021/acsanm.9b01641).
- 34 S. Danilova, J. E. Graves, J. Sort, E. Pellicer, G. W. V. Cave and A. Cobley, Electroless copper plating obtained by Selective Metallisation using a Magnetic Field (SMMF), *Electrochim. Acta*, 2021, **389**, 138763, DOI: [10.1016/j.electacta.2021.138763](https://doi.org/10.1016/j.electacta.2021.138763).
- 35 M. Aleem, R. Vishnuraj, B. Krishnan and B. Pullithadathil, Realization of Micropatterned, Narrow Line-Width Ni-Cu-Sn Front Contact Grid Pattern Using Maskless Direct-Write Lithography for Industrial Silicon Solar Cells, *ACS Appl. Energy Mater.*, 2021, **4**(10), 10682–10696, DOI: [10.1021/acsanm.1c01699](https://doi.org/10.1021/acsanm.1c01699).
- 36 R. G. Milazzo, *et al.*, Influence of hydrofluoric acid treatment on electroless deposition of Au clusters, *Beilstein J. Nanotechnol.*, 2017, **8**, 183–189, DOI: [10.3762/bjnano.8.19](https://doi.org/10.3762/bjnano.8.19).
- 37 S. Y. Sayed, F. Wang, M. Malac, A. Meldrum, R. F. Egerton and J. M. Buriak, Heteroepitaxial Growth of Gold Nanostructures on Silicon by Galvanic Displacement, *ACS Nano*, 2009, **3**(9), 2809–2817, DOI: [10.1021/nn900685a](https://doi.org/10.1021/nn900685a).
- 38 J. Fang, H. You, P. Kong, Y. Yi, X. Song and B. Ding, Dendritic Silver Nanostructure Growth and Evolution in Replacement Reaction, *Cryst. Growth Des.*, 2007, **7**(5), 864–867, DOI: [10.1021/cg0604879](https://doi.org/10.1021/cg0604879).
- 39 F. Gentile, *et al.*, Electroless deposition dynamics of silver nanoparticles clusters: A diffusion limited aggregation (DLA) approach, *Microelectron. Eng.*, 2012, **98**, 359–362, DOI: [10.1016/j.mee.2012.07.041](https://doi.org/10.1016/j.mee.2012.07.041).
- 40 W.-W. Hu, S.-Y. Yang, C.-W. Tsao, S.-L. Chen and C.-Y. Tzeng, Deposition of polypyrrole on wrinkled polydimethylsiloxane to fabricate stretchable conductive membranes for multifunctional bioreactor applications, *Prog. Org. Coat.*, 2023, **181**, 107573, DOI: [10.1016/j.porgcoat.2023.107573](https://doi.org/10.1016/j.porgcoat.2023.107573).
- 41 K. Peng, A. Lu, R. Zhang and S.-T. Lee, Motility of Metal Nanoparticles in Silicon and Induced Anisotropic Silicon Etching, *Adv. Funct. Mater.*, 2008, **18**(19), 3026–3035, DOI: [10.1002/adfm.200800371](https://doi.org/10.1002/adfm.200800371).
- 42 Y.-T. Lu and A. R. Barron, Anti-reflection layers fabricated by a one-step copper-assisted chemical etching with inverted pyramidal structures intermediate between texturing and nanopore-type black silicon, *J. Mater. Chem. A*, 2014, **30**(2), 12043–12052, DOI: [10.1039/C4TA02006E](https://doi.org/10.1039/C4TA02006E).
- 43 K. Gao, *et al.*, Fabrication of black silicon by Ni assisted chemical etching, *Mater. Res. Express.*, 2018, **5**(1), 015020, DOI: [10.1088/2053-1591/aaa1fb](https://doi.org/10.1088/2053-1591/aaa1fb).

